$H(t)$ being the unit step function, while G represents the normalized boundary layer structure. This type of boundary layer is very suitable to check the present method experimentally and to investigate the effect of the internal reflections. The experimental setup is sketched in Fig. 1. The plane of polarization of the helium-neon laser beam is chosen parallel to the plane of incidence. The light beam reflecting from the outer surface of the shock tube window is used as a reference to reduce the effect of laser instabilities. The electronic circuit has a rise time less than 2.10^{-7} sec. In Fig. 2 some experimental and theoretical results are shown for the case of shock reflection in argon for different shock Mach numbers M, initial pressures p_0, and angles of incidence θ_0. Initially, the jump in direct reflection is compensated completely by the internal reflections inside the infinitely thin boundary layer. As the boundary layer grows, the internal reflections vanish and asymptotically a change in reflectivity is observed proportional to $(n_s - n_0)$. The solid curves show the theoretical predictions based on the substitution of a somewhat simplified boundary layer solution into Eqs. (1, 6, and 8).

The agreement is very satisfactory. The systematic deviation between theory and experiment for the lowest pressure is due to the phenomenon of temperature jump between gas and wall.

It is concluded from these experiments that the change in refractive index $(n_s - n_0)$ can be derived from the final change in reflectivity when the boundary layer thickness has become sufficiently large. This has been applied to study the influence of thermal diffusion in a thermal boundary layer in a mixture of argon and helium.[3] A separation of species could be shown by a measurement of the refractive index at the wall.

Viscous Side-Wall Boundary Layer

As a last example, we will discuss an application to the sidewall of a shock tube. At the passage of a shock wave the refractive index at the wall undergoes a jump proportional to the change in pressure. After some time the contact region will pass, separating driver and test gas.

Figure 3 shows the reproduction of an oscilloscope recording for an experiment with nitrogen as test gas and hydrogen as driver. The upper curve is obtained from the change in reflectivity, which is now proportional to $(n_s - n_0)$ since internal reflections can be completely neglected. The lower curve shows the pressure, measured with a piezoelectric transducer. The arrow indicates the arrival of the contact region, when the reflectivity signal starts decreasing due to the lower refractive index of hydrogen compared with nitrogen. After the passage of the reflected shock wave in hydrogen, expansion waves cause a decay in refractive index and in pressure. The experiment illustrates that the reflectivity method offers the possibility of distinguishing between different gases and can provide additional information on the state of a gas at a wall.

Acknowledgment

The author is indebted to J.F.H. Willems, H.J. Jager, and L.J.M. Haffmans for their experimental contributions.

References

[1] Jacobsson, R., "Light Reflection from Films of Continuously Varying Refractive Index," *Progress in Optics,* Vol. 5, North Holland Publishing Cie., Amsterdam, 1966, pp. 249-286.

[2] Clarke, J.F., "The Reflexion of a Plane Shock Wave from a Heat Conducting Wall," *Proceedings of the Royal Society,* A, Vol. 299, 1967, pp. 221-237.

[3] van Dongen, M.E.H., van Gils, J.F.M., Willems, J.F.H., and Vossers, G., "Thermal Diffusion in the End Wall Thermal Boundary Layer of a Shock Tube," *Proceedings of the Xth International Shock Tube Symposium,* Shock Tube Research Society, Japan, 1975, pp. 119-126.

Low Reynolds Number Flow Past a Blunt Axisymmetric Body at Angle of Attack

Ajay Kumar*
NASA Langley Research Center, Hampton, Va.

Nomenclature

C_D = total drag coefficient based on the local base area
C_{D_p} = pressure drag coefficient based on the local base area
c_f = skin-friction coefficient
c_H = heat-transfer coefficient, $\dot{q}'_w / \frac{1}{2}\rho'_\infty V'^3_\infty$
h = specific enthalpy, h'/V'^2_∞
n = normal coordinate, n'/R'_N
p = pressure, $p'/\rho'_\infty V'^2_\infty$
r = local body radius, r'/R'_N
R'_N = nose radius
Re = freestream Reynolds number, $\rho'_\infty V'_\infty R'_N/\mu'_\infty$
s = tangential coordinate, s'/R'_N
u = tangential velocity, u'/V'_∞
U_s = shock speed, U'_s/V'_∞
v = normal velocity component, v'/V'_∞
V'_∞ = freestream velocity
V_{N_∞} = freestream velocity normal to the shock, V'_{N_∞}/V'_∞
V_{T_∞} = freestream velocity tangential to the shock, V'_{T_∞}/V'_∞
ρ = density, ρ'/ρ'_∞
μ = viscosity, μ'/μ'_∞
γ = ratio of specific heats
α = angle of attack

Subscripts

N = conditions behind the shock
w = conditions at the body surface
∞ = conditions in the freestream

Superscript

$'$ = dimensional quantities

Introduction

THE problem of computing the laminar hypersonic flow at low Reynolds numbers past blunt axisymmetric bodies has been investigated by many authors[1-3] using viscous shock-layer equations or full Navier-Stokes equations; however, these investigations are limited to zero angle of attack. The purpose of this Note is to investigate the low Reynolds number flow of a perfect gas over a blunt axisymmetric body of large half-angle at small angles of attack, which represents the conditions encountered by the planetary entry probes during the early (high-altitude) portions of an atmospheric entry trajectory. Time-dependent viscous shock-layer equations are used to describe the flowfield. These equations are obtained from the full Navier-Stokes equations by keeping terms up to second order in the inverse square root of Reynolds number in both the viscous and inviscid regions. The equations are valid for moderate to high Reynolds numbers. A time asymptotic finite-difference method is used to solve these equations in the plane of symmetry of the flowfield. Since the crossflow velocity is identically zero in the plane of symmetry, the crossflow momentum equation cannot be used directly. The required equation is obtained by dif-

Received March 24, 1977.
Index categories: Viscous Nonboundary-Layer Flows; Supersonic and Hypersonic Flow.

*Postdoctoral Research Associate, National Research Council, Washington, D.C., working in the Computational Fluid Dynamics Group, Aerothermodynamics Branch, Space Systems Division. Member AIAA.

ferentiating the momentum equation with respect to the crossflow direction, and the crossflow velocity gradient then is used as the new dependent variable. The meridional variation in pressure is required in the analysis. It is expressed as the cosine function of the crossflow direction as given in Ref. 4. The flow properties on the body surface are given by the velocity slip and temperature jump conditions, whereas a set of shock slip conditions is used to determine the flow properties behind the shock.

Various flow quantities such as drag coefficient, skin friction coefficient, and heating rates are obtained at zero and small angles of attack. The drag coefficients for the zero-angle-of-attack case are compared with the experimental results of Little.[5] No results were available for comparison with the present results at angle of attack. The effect of slip conditions on various flow quantities also is discussed.

Governing Equations and Method of Solution

The governing equations, assumptions, and overall approach used in the present analysis are given in Ref. 4. However, the boundary conditions now are modified so as to include the low Reynolds number effects. The slip boundary conditions at the body surface are given in Ref. 1. The constants appearing in those relations are taken from Ref. 6.

The flow properties behind the shock wave are obtained by modifying the shock relations, given in Ref. 7, for velocity and temperature gradients behind the shock wave. The shock speed U_s now is given by

$$U_s = V_{N_\infty} + (d_1 + \sqrt{d_1^2 - 4' d_2})/2 \tag{1}$$

where

$$d_1 = k_2/k_3, \qquad d_2 = [k_1^2 + (p_N - p_\infty)\left(\frac{\gamma+1}{\gamma-1} p_N + p_\infty\right)]/2k_3$$

$$k_1 = \left(\mu \frac{\partial u}{\partial n}\right)_N / Re$$

$$k_2 = \left(\mu \frac{\partial h}{\partial n}\right)_N / PrRe$$

$$k_3 = (p_\infty - p_N)/(\gamma - 1)$$

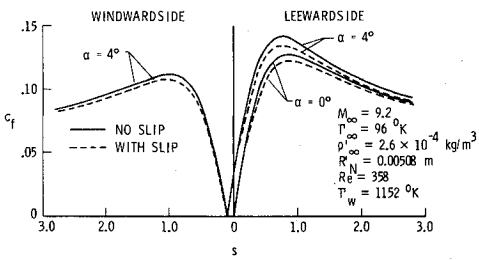

Fig. 1 Skin-friction coefficient distribution on a 90° hyperboloid at $\alpha = 0°$ and 4°.

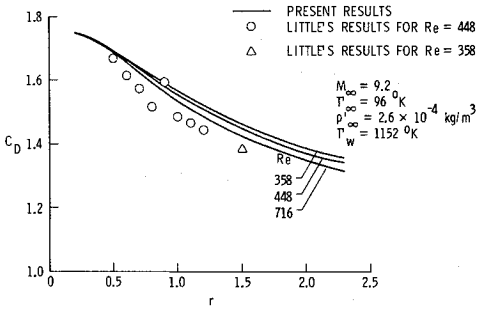

Fig. 2 Comparison of drag coefficient for a 90° hyperboloid at $\alpha = 0°$.

Knowing the value of U_s, other flow properties are obtained from the relations

$$u_N = V_{T_\infty} + k_1/(V_{N_\infty} - U_s) \tag{2}$$

$$v_N = (p_\infty - p_N)/(V_{N_\infty} - H_\lambda) + \Psi_\infty \tag{3}$$

$$\rho_N = (V_{N_\infty} - U_s)/(v_N - U_s) \tag{4}$$

Here u_N and v_N are defined with respect to the shock wave. These can be resolved suitably to give the flow velocity behind the shock wave in body-oriented coordinates.

MacCormack's[8] two-step finite-difference method is used to solve the governing equations. The details are given in Ref. 4. The only difference is that, in the present analysis, the shear stress and heat flux terms are calculated by using backward differencing in the predictor step and forward differencing in the corrector step. The fourth-order damping, used in the present calculations, requires a damping coefficient of 0.003.

Results and Discussion

Flowfield calculations are made for a 90° hyperboloid at angles of attack of 0°, 4°, and 8°. Zero-angle-of-attack results are obtained at the freestream Reynolds numbers of 358, 448, and 716, whereas the angle-of-attack results are obtained at a freestream Reynolds number of 358 only. In all of the cases, freestream Mach number is 9.2

Figure 1 shows the distribution of skin-friction coefficient with and without slip conditions at $\alpha = 0°$ and 4°. It is seen that the slip reduces the skin-friction coefficient by about 5% in the nose region, and the reduction decreases for the downstream points. It also is seen that the effect of slip is slightly higher on the leeward side than on the windward side.

In Fig. 2, the total drag coefficient is plotted against the local body radius at $\alpha = 0°$. Pressure jump on the surface is included in calculating the drag coefficient. It is seen that the drag coefficient increases with the decrease in the Reynolds number for a given body. Experimental results of Little[5] also are plotted. The present results are about 5% higher than the experimental results. Little[5] estimates his possible experimental error in drag at about ±7%. The present results are, in general, within these limits.

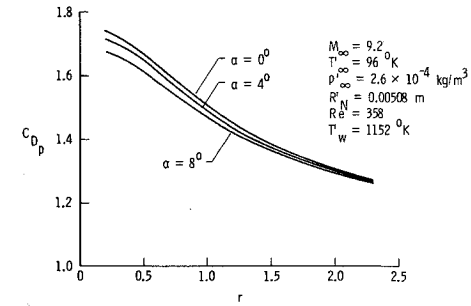

Fig. 3 Effect of angle of attack on the pressure drag for a 90° hyperboloid.

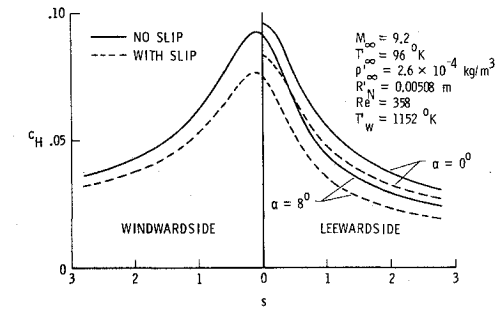

Fig. 4 Heating rate distribution on a 90° hyperboloid at $\alpha = 0°$ and 8°.

Figure 3 shows the effect of angle of attack on the pressure drag coefficient at a given Reynolds number. Again, the pressure jump on the surface is included. It is seen that the effect of the angle of attack is to reduce the pressure drag for a given body. The reduction in the drag increases as the bluntness of the body increases.

In Fig. 4, the heating rate results are plotted with and without slip conditions at $\alpha = 0°$ and 8°. The effect of slip is to reduce the heating rates. The magnitude of the difference is maximum in the nose region of the body and decreases for the downstream points.

References

[1] Davis, R.T., "Numerical Solution of the Hypersonic Viscous Shock Layer Equations," *AIAA Journal*, Vol. 8, May 1970, pp. 843-851.

[2] Scott, C.D., "Reacting Shock Layers With Slip and Catalytic Boundary Conditions," *AIAA Journal*, Vol. 13, Oct. 1975, pp 1271-1278.

[3] Li, C.P., "Hypersonic Nonequilibrium Flow Past a Sphere at Low Reynolds Numbers," AIAA Paper 74-173, Washington, D.C., 1974.

[4] Kumar, A. and Graves, R.A., Jr., "Numerical Solution of the Viscous Hypersonic Flow Past Blunted Cones at Angle of Attack," AIAA Paper 77-172, Los Angeles, Calif., 1977.

[5] Little, H.R., "An Experimental Investigation of Surface Conditions on Hyperboloids and Paraboloids at a Mach Number of 10," M.S. Thesis, Univ. of Tennessee, 1969.

[6] Srivastava, B.N., Davis, R.T., and Werle, M.J., "Slip Model for Hypersonic Viscous Flows," *AIAA Journal*, Vol. 14, Feb. 1976, pp. 257-259.

[7] Xerikos, J. and Anderson, W.A., "A Time-Dependent Approach to the Numerical Solution of the Flow Field About an Axisymmetric Vehicle at Angle of Attack," NASA CR-61982, 1968.

[8] MacCormack, R.W., "The Effect of Viscosity in Hypervelocity Impact Cratering," AIAA Paper 69-354, Cincinnati, Ohio, 1969.

Technical Comments

Comment on "Discretized Simulation of Vortex Sheet Evolution with Buoyancy and Surface Tension Effects"

James W. Rottman* and D. B. Olfe†
University of California at San Diego, La Jolla, Calif.

ZALOSH[1] carried out calculations for the roll-up of a vortex sheet separating inviscid fluids of different densities. The derivation of his Eq. (14) for the rate of change of circulation following a discrete vortex contains an error that results in the omission of a term from the equation. For a continuous vortex sheet without surface tension effects, the correct expression for the rate of change of circulation per unit length was given in an earlier paper by Zaroodny and Greenberg.[2] Zalosh's numerical results probably would be little changed by the use of the correct equation, because his calculations were for small density differences, and the omitted term is proportional to the density difference across the vortex sheet. On the other hand, use of Zalosh's equation for a problem involving large density differences would result in large errors.

The error of Ref. 1 involves the convective part of the total (Lagrangian) derivative. Proper care was not taken in distinguishing between derivatives following fluid particles on either side of the vortex sheet and the derivative following the vortex motion. The rate of change of circulation following a closed circuit C moving with the fluid is given by[3]

$$\frac{d\Gamma}{dt} = \frac{d}{dt}\int_{(C)} \boldsymbol{V}\cdot d\boldsymbol{r} = \int_{(C)} \frac{d\boldsymbol{V}}{dt}\cdot d\boldsymbol{r} + \int_{(C)} \boldsymbol{V}\cdot d\left(\frac{d\boldsymbol{r}}{dt}\right) \tag{1}$$

Received Jan. 31, 1976.
Index categories: Hydrodynamics; Subsonic Flow; Transonic Flow.

*Graduate Student, Department of Applied Mechanics and Engineering Sciences.

†Professor, Department of Applied Mechanics and Engineering Sciences. Associate Fellow AIAA.

Because the Lagrangian derivative follows the fluid particles, $d\boldsymbol{r}/dt = \boldsymbol{V}$, and the last integral in Eq. (1) vanishes. Consider a closed circuit centered at a position s_i on a vortex sheet, and having sides of length ℓ just above and below the sheet. The rate of change of (clockwise) circulation around the vortex sheet segment is

$$\frac{d\Gamma_i}{dt} = \int_{s_i-\ell/2}^{s_i+\ell/2} \left[\left(\frac{d\boldsymbol{V}_1}{dt}\right)_s - \left(\frac{d\boldsymbol{V}_2}{dt}\right)_s\right] ds \tag{2}$$

where $\boldsymbol{V}_1$ and $\boldsymbol{V}_2$ denote the velocities just above and below the vortex sheet, the subscript s denotes the components tangential to the vortex sheet, and ds is the differential distance along the sheet. Equation (2) has the same form as Eq. (7) of Ref. 1, provided that we interpret Zalosh's terms $d\boldsymbol{V}_{1s}/dt$ and $d\boldsymbol{V}_{2s}/dt$ as the tangential components of the accelerations, i.e., as $(d\boldsymbol{V}_1/dt)_s$ and $(d\boldsymbol{V}_2/dt)_s$, respectively. However, contrary to the statement by Zalosh, the Lagrangian derivatives follow the fluid particles, not the ith vortex; i.e.,

$$(d\boldsymbol{V}_1/dt)_s \equiv (\partial \boldsymbol{V}_1/\partial t)_s + (\boldsymbol{V}_1\cdot\nabla\boldsymbol{V}_1)_s$$

$$(d\boldsymbol{V}_2/dt)_s \equiv (\partial \boldsymbol{V}_2/\partial t)_s + (\boldsymbol{V}_2\cdot\nabla\boldsymbol{V}_2)_s$$

The momentum equation [Eq. (8) in Ref. 1] is used to determine the acceleration terms in Eq. (2)

$$\left(\frac{d\boldsymbol{V}_1}{dt}\right)_s = -\frac{1}{\rho_1}\frac{\partial p_1}{\partial s} - g\sin\theta, \quad \left(\frac{d\boldsymbol{V}_2}{dt}\right)_s = -\frac{1}{\rho_2}\frac{\partial p_2}{\partial s} - g\sin\theta \tag{3}$$

where again the total derivatives follow fluid particles in the upper and lower fluids, respectively. Substitution of Eqs. (3) into Eq. (2) yields Zalosh's Eq. (9), which is correct.

The velocity of a vortex is given as the average of the fluid velocities above and below; i.e., $\boldsymbol{V}_i = \frac{1}{2}(\boldsymbol{V}_1 + \boldsymbol{V}_2)$. Differentiation following the vortex yields an equation of the form of Eq. (12) of Ref. 1:

$$\left(\frac{d\boldsymbol{V}_i}{dt}\right)_s = \frac{1}{2}\left[\left(\frac{d\boldsymbol{V}_1}{dt}\right)_s + \left(\frac{d\boldsymbol{V}_2}{dt}\right)_s\right] \tag{4}$$